Electronic Supplementary Information

Motile bacteria crossing liquid-liquid interfaces of an aqueous isotropic-nematic coexistence phase

Jiyong Cheon, Joowang Son, Sungbin Lim, Yundon Jeong, Jung-Hoon Park, Robert J. Mitchell, Jaeup U. Kim, and Joonwoo Jeong

Description of Supplementary Movies

- **Movie S1:** Motile *Bacillus subtilis* dispersed in the isotropic-nematic coexistence phase with multiple interfaces. All bacteria in this large field of view are in focus, suggesting that this is a quasi-2D system. Scale bar = 50 μm
- **Movie S2:** *Bacillus subtilis* is crossing the liquid-liquid interface. Scale bar = 20 μm. The trajectory shows the positions of the moving front.
- **Movie S3:** *Bacillus subtilis* is trapped at the liquid-liquid interface. Scale bar = 20 μm. The trajectory shows the positions of the moving front.
- **Movie S4:** *Bacillus subtilis* with fluorescently-labeled flagella crossing the liquid-liquid interface. Scale bar = 5 μm.
- **Movie S5:** *Bacillus subtilis* with fluorescently-labeled flagella swimming in the isotropic phase is shown in a body-centered frame of reference. The arrow indicates the swimming direction. Scale bar = 2 μm.
- **Movie S6:** *Bacillus subtilis* with fluorescently-labeled flagella swimming in the nematic phase is shown in a body-centered frame of reference. The arrow indicates the swimming direction. Scale bar = 2 μm.

Supplementary Data

Analysis of angles between bacteria and interfaces

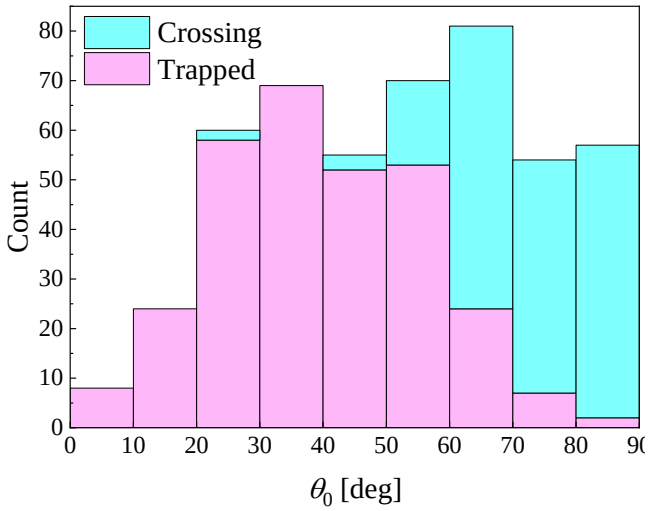

Figure S1: Stack histogram of all incident angles of *Bacillus subtilis* encountering the isotropic-nematic interface from the isotropic phase. We present the same data set used in Fig. 2(c): $N = 180$ (crossing) and $N = 297$ (trapped).

We investigated 477 bacteria encountering the interface from the isotropic phase and found no preferred angle but a rather uniform distribution, as shown in Fig. S1. Namely, except for the very shallow angles, the total counts for various incident angles are similar, while the crossing behavior strongly depends on the incident angle. Figure S2 shows how bacteria rotate as they move and interact with the isotropic-nematic interfaces. The angles of bacteria that successfully cross the interface typically decrease, as shown in Figs. S2(a, c-d). The angles of the trapped bacteria also decrease and converge to 0, *i.e.*, parallel to the interface.

Crossing behavior's dependencies on other motility parameters

As shown in Fig. S4, we find no apparent correlations between crossing behavior and other motility parameters but the incident angle (see Fig. 2(c)) and the normal propulsion force, in which the incident angle contributes.

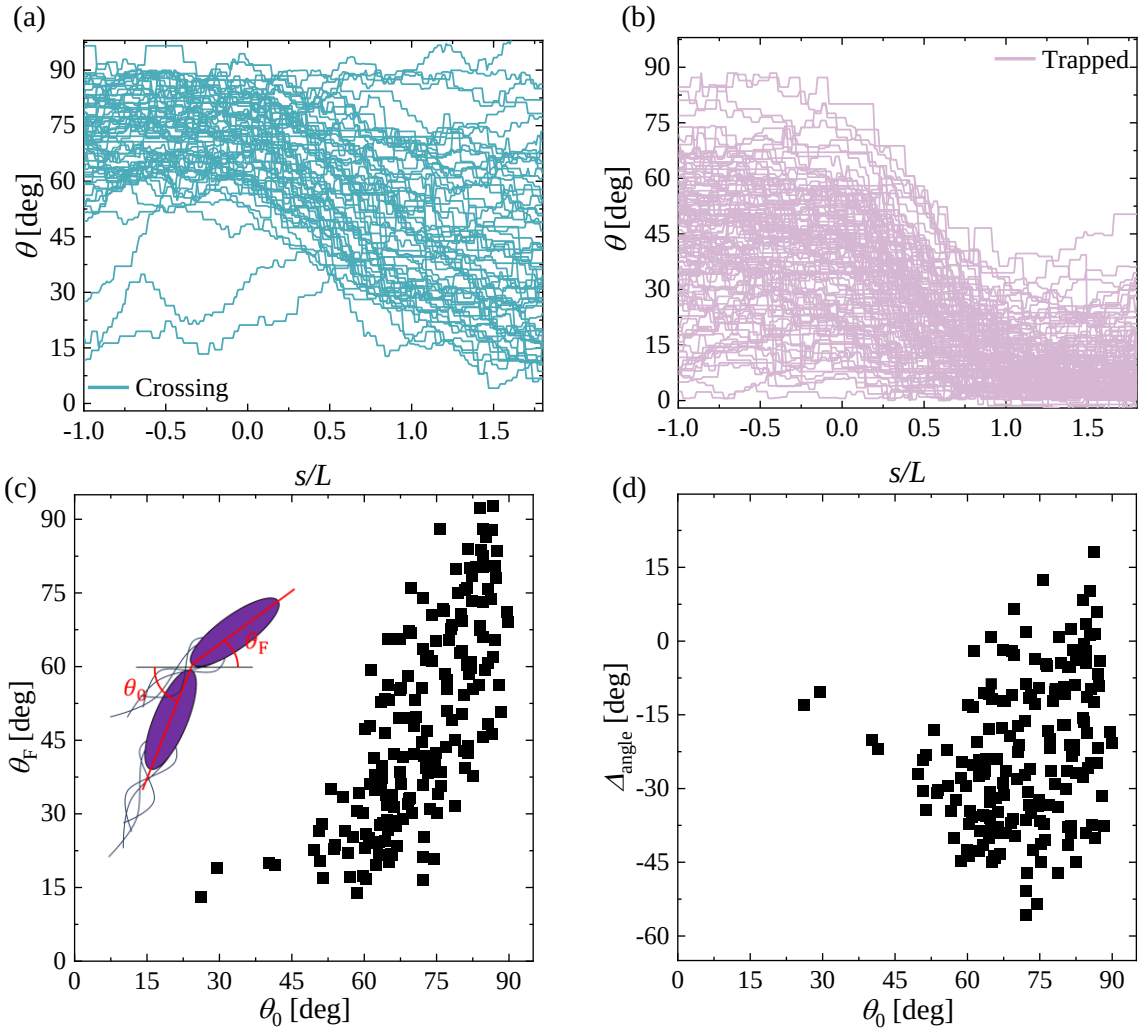

Figure S2: Rotation of the bacteria interacting with the interface. (a) and (b) Change of the angle between bacteria and interfaces as a function of normalized travel distance. An individual trajectory is from a bacterium (a) crossing the interface and (b) being trapped at the interface. We present the same data set used in Figs. 2(a-b, d-e): $N = 63$ (crossing) and $N = 119$ (trapped)). (c) The angle before and after crossing interfaces ($N = 180$, the data set used in Fig. 2(c)). The incident angle is the angle when a bacterium meets the interface, and the final angle is estimated when the bacterium swims its body length after breaching the interface, as sketched in the inset. (d) The change in the angle, $\Delta_{\text{angle}} = \theta_{\text{F}} - \theta_0$, as a function of the incident angle.

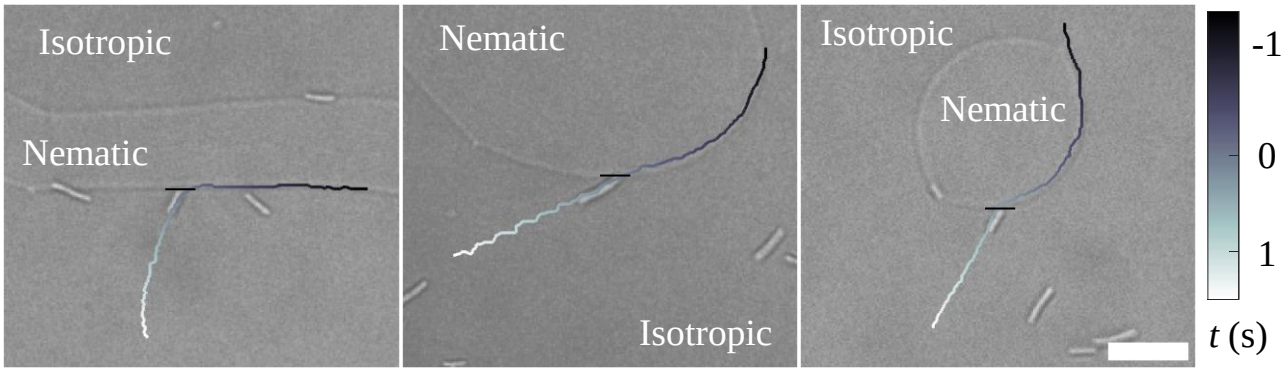

Figure S3: Three representative trajectories are plotted on optical micrographs with curved isotropic-nematic interfaces. A short horizontal black line around the center of each image corresponds to the tangential line of the interfaces at which a bacterium starts to interact with the interface. The trajectory color codes indicate the time from when the bacterium touches the interface. Scale bar = 20 μm

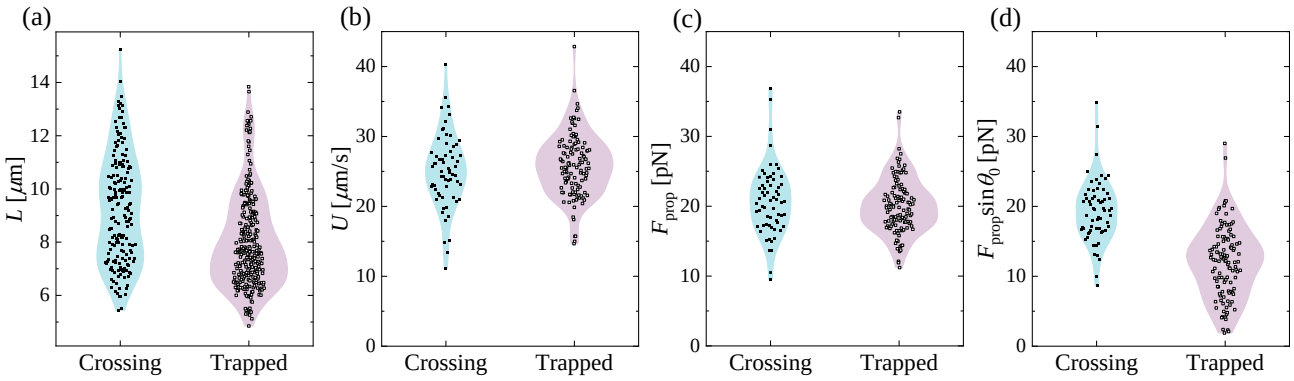

Figure S4: Crossing behavior's dependencies on other motility parameters: (a) body length, (b) incident speed, (c) propulsion force, and (d) propulsion force normal to the interface. The data in (a) is from the data set used in Fig. 2(c): $N = 180$ (crossing) and $N = 297$ (trapped), while the data in (b), (c), and (d) are from the data set used in Figs. 2(a-b): $N = 63$ (crossing) and $N = 119$ (trapped).

Estimation of the interfacial tension by the tactoid method

Applying the tactoid method introduced in Ref. 47 of the main text (Paparini and Virga), we estimate the interfacial tension of the water-water interface in the isotropic-nematic coexistence phase. In Ref. 47, a tactoid with an aspect ratio = 1.3 and $\tau_{\mathrm{N}} = 1.99$ rad gives 8.9 μN/m. Our tactoid shown in Fig. S5 has a similar shape and has a similar interfacial tension of the order of 10 μN/m: The measured aspect ratio and τ_{N} are 1.2 and 2.1 rad, respectively.

Specifically, the interfacial tension $\gamma = \frac{\alpha K_{11}}{R_e}$ is determined using the reduced area α, the splay elastic constant K_{11}, and the equivalent radius of the tactoid R_{e}. Utilizing the measured geometric parameters, including aspect ratio and τ_N, and Fig. 11 in Ref. 47, we find $\alpha \approx 29$ and $R_{\mathrm{e}} \approx 20$ μm. As in Ref. 47, since the measurement of the elastic moduli of the nematic phase in the coexistence phase is not available, we adopt the order-of-magnitude estimation of K_{11} from the fully nematic phase, which is 10 pN. Consequently, the best order-of-magnitude estimation for the interfacial tension of our interface is 10 μN/m.

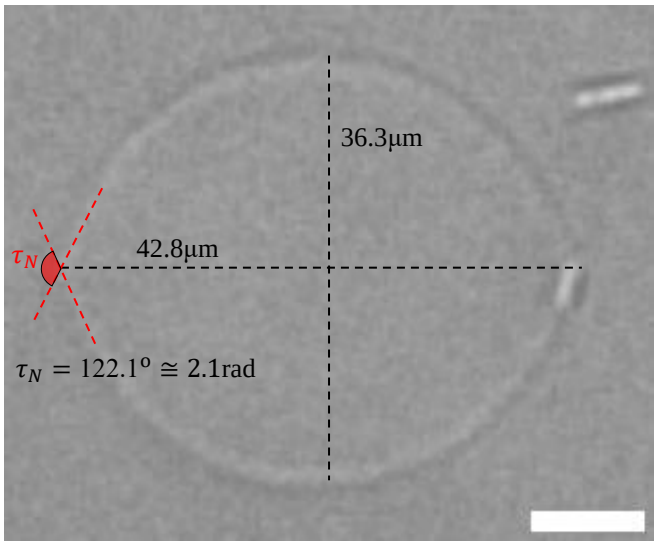

Figure S5: A geometric analysis of a representative nematic tactoid surrounded by the isotropic phase in our quasi-2D cell. The black dotted lines represent the major and minor axes, and the red dotted lines correspond to the tangential lines at the cusp. τ_{N} is the angle between two red lines. The scale bar is 10 μm.

The near 90-deg contact angle between the isotropic-nematic interface and *B. subtilis*

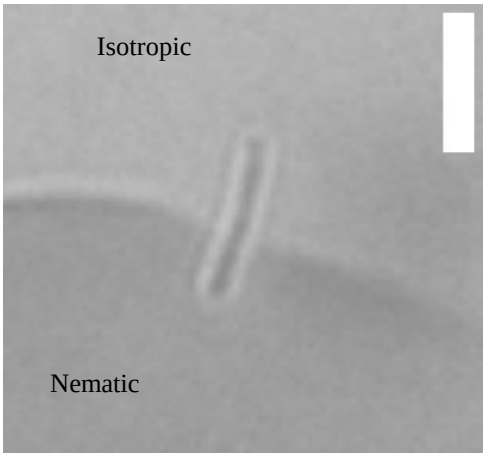

Figure S6: The 90-deg contact angle between the isotropic (I)-nematic (N) interface and immotile *B. subtilis*. Scale bar = 10 μm

There exist immotile *B. subtilis* in the sample, possibly because they were stuck to the substrates. We find several immotile bacteria lying across the isotropic-nematic interface and discover that they all have a near 90-degree contact angle to the interface, as shown in Fig. S6. This indicates that *B. subtilis* do not have an affinity to a specific phase, *i.e.*, like each phase equally. This enables us to exclude affinity-related forces and assume that the interfacial tension and critical deformation of the interface determine the crossing behavior.

Derivation of equations of motion

The ellipsoid in Fig. 3(b) is our model bacterium, which swims in the $x-y$ plane. We use the contour-length coordinate s along which the center of the ellipsoid moves and assume the major axis of the ellipsoid is parallel to the tangential direction of the swimming path.

When the ellipsoid touches the interface parallel to the x direction at time $t = 0$, the interface starts to deform and exert a force on the tip of the ellipsoid along the y direction, which is normal to the interface. We assume this force $F_{\text{interface}}$ is $c\gamma\Delta_{\text{int}}$ with the interfacial tension γ, interfacial deformation Δ_{int}, and a proportional coefficient c, which is set to 1 considering that we use the order-of-magnitude estimation of γ. This force competes with the propulsion force F_{prop} and induces the rotation of the ellipsoid.

The overdamped equations of motion regarding the translational motion of the ellipsoid is

$$0 = F_{\text{prop}} - \mu_{\text{trans}}\frac{ds_{\text{B}}(t)}{dt} - F_{\text{interface}}\sin\theta(t), \tag{S1}$$

where the translation drag coefficient μ_{trans} of the ellipsoid along the major axis is $\frac{4\pi\eta a}{\ln(\frac{2a}{b})-\frac{1}{2}}$ with the semi-major and semi-minor axes, a and b, respectively. The rotational motion is similarly governed by

$$0 = aF_{\text{interface}}\cos\theta(t) - \mu_{\text{rot}}\frac{d\theta(t)}{dt}, \tag{S2}$$

where the rotational drag coefficient μ_{rot} of the ellipsoid about the minor axis is $\frac{8\pi\eta a^3/3}{\ln(\frac{2a}{b})-\frac{1}{2}}$. Utilizing $ds\sin\theta = dy$, we multiply $\sin\theta$ on both sides of Eqs. (S1) and (S2) and derive Eqs. (1) and (2) of the main text.

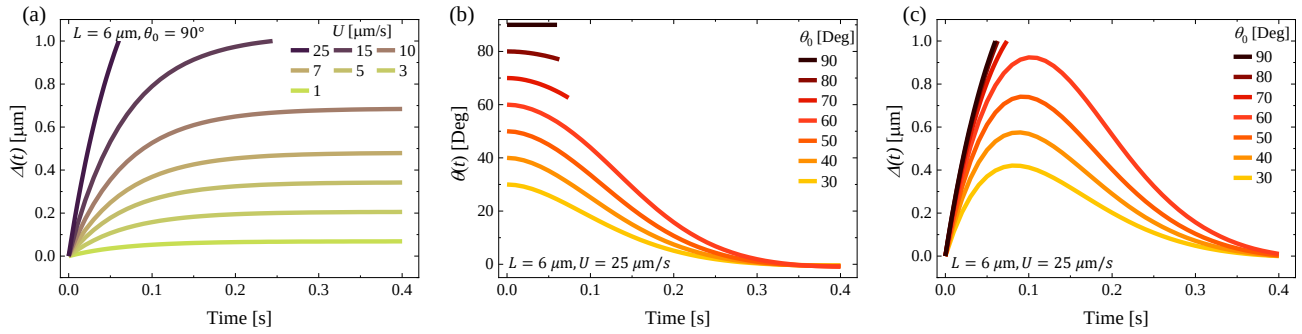

Figure S7: Representative numerical solutions of Eqs. S1 and S2 depend on parameters. All calculations are performed when $\Delta(t) \leq 1$ μm, *i.e.*, before breaching the interface. (a) The interfacial deformation $\Delta(t) = y_{\text{B}} + a\sin\theta(t)$ depending on the swimming speed U when $\theta_0 = 90$ deg and $L = 6$ μm. (b) and (c) The orientation of bacterium body $\theta(t)$ and the interfacial deformation $\Delta(t)$ depend on θ_0 when $U = 25$ μm/s and $L = 6$ μm.

Comparison between experimental data and model calculation: Incident angle and speed

The experimental data set in Fig. 3(c) is shown again with model predictions according to the incident angle θ_0 and speed U. Most triangles are located in the upper gray regions with higher incident angles, whereas the limited U-range and various body lengths L give no clear evidence of U-dependencies.

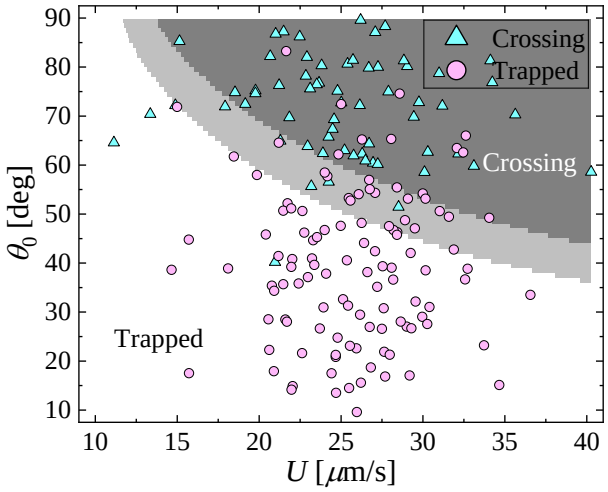

Figure S8: The comparison between experimental data and model calculation according to the incident angle and speed. Each data point is from the observation of an individual bacterium. The model calculation results divide the background regions. The top gray region corresponds to the condition for a model bacterium to cross the interface when its body length is longer than 10.0 μm. The bottom white region is when the bacteria fail to cross the interface when its body length is shorter than 6.1 μm. Here we present the data set used in Figs. 2(a) and (b): $N = 63$ (crossing) and $N = 119$ (trapped), respectively.

Analysis of wiggling trajectories

We first estimated baselines from the trajectories to find the wiggling angle ϕ. Fig. S9(a) shows a wiggling trajectory in the time domain. After identifying local extrema, we defined the baseline by interpolating midpoints between adjacent local maximum and minimum, as shown in Fig. S9(b). Subtracting the baseline from $\theta(t)$ in Fig. S9(a) gives $\delta\theta(t)$. We applied the same method for Fig. 4(a). We analyzed the $\delta\theta$ curves in spatiotemporal domains to determine the wiggling angle, pitch, and frequency.

FigureS10 shows how bacteria wiggling differs between the isotropic and nematic phases. Average values in each phase are $\phi_{\mathrm{I}} = 3.7 \pm 1.7$ deg, $\phi_{\mathrm{N}} = 2.9 \pm 1.0$ deg, $\mathrm{frequency}_{\mathrm{I}} = 4.6 \pm 1.5$ Hz, $\mathrm{frequency}_{\mathrm{N}} = 6.4 \pm 1.8$ Hz, $\mathrm{pitch}_{\mathrm{I}} = 5.5 \pm 1.1$ μm, and $\mathrm{pitch}_{\mathrm{N}} = 4.4 \pm 1.2$ μm. A clear distinction with smaller wiggling angle but faster frequency is observed in swimming in the nematic phase with respect to the isotropic phase.

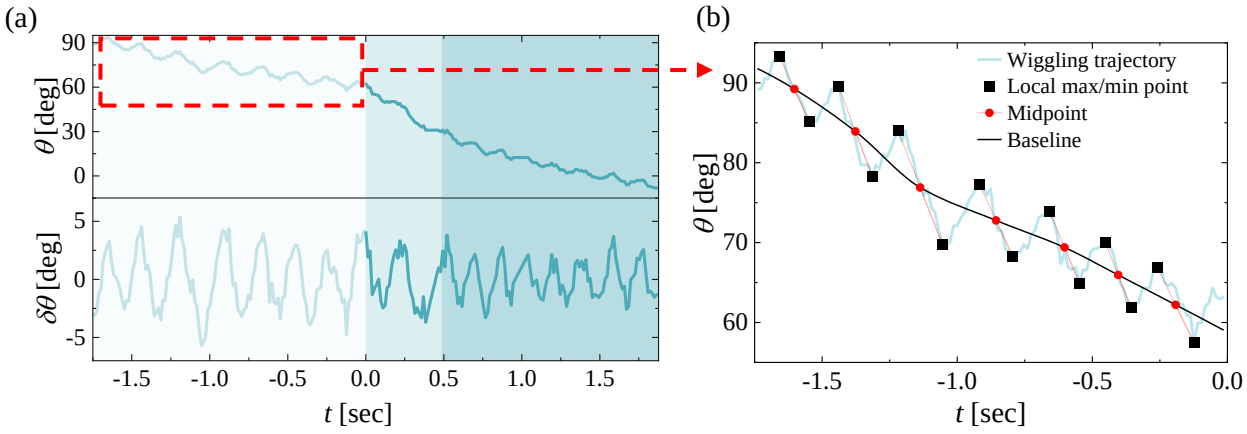

Figure S9: Analysis of a wiggling trajectory in the time domain. (a) A representative wiggling trajectory before and after baseline subtraction. The top graph shows the angle θ between the body and interface as a function of time t, while the bottom plots $\delta\theta$ after the baseline subtraction. The same trajectory in the spatial domain is shown in Fig. 4(b). The shaded backgrounds are provided to help distinguish the phases in which a bacterium is located. (b) Estimation of the baseline. The data within the red box of (a) is magnified here. The black squares indicate the local minima/maxima of $\theta(t)$, and the red circles between the connected squares are their midpoints. Interpolating the red circles into a solid black line gives the baseline.

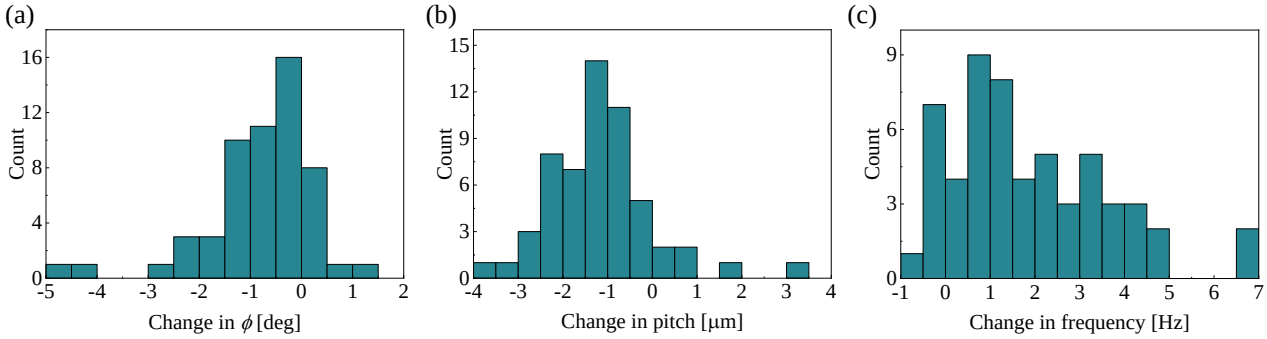

Figure S10: Changes in wiggling angle ϕ, frequency, and pitch as the bacteria enter the nematic phase from the isotropic phase. We analyzed 56 trajectories out of the 63 shown in Fig. S2.

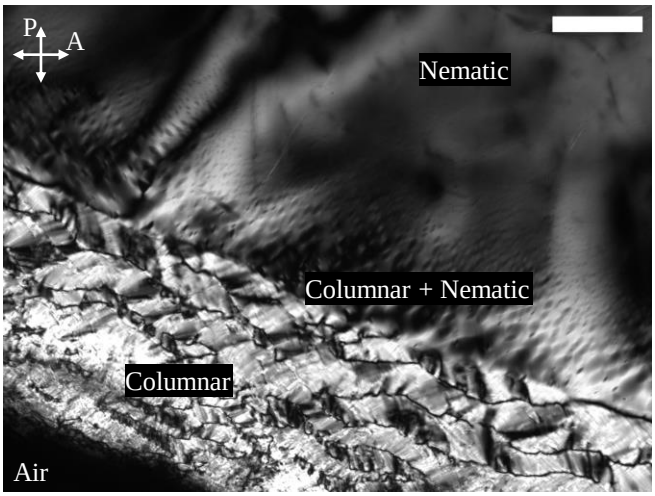

Figure S11: A representative polarized optical microscopy image showing the nematic and columnar phases simultaneously. This is the same TB-DSCG specimen used in the bacterial experiments but at room temperature. It is not sealed on purpose, and the resulting evaporation of water leads to the formation of a columnar phase at higher concentrations. Note that the columnar phase exhibits a unique optical texture populated with defects. Scale bar = 100 μm

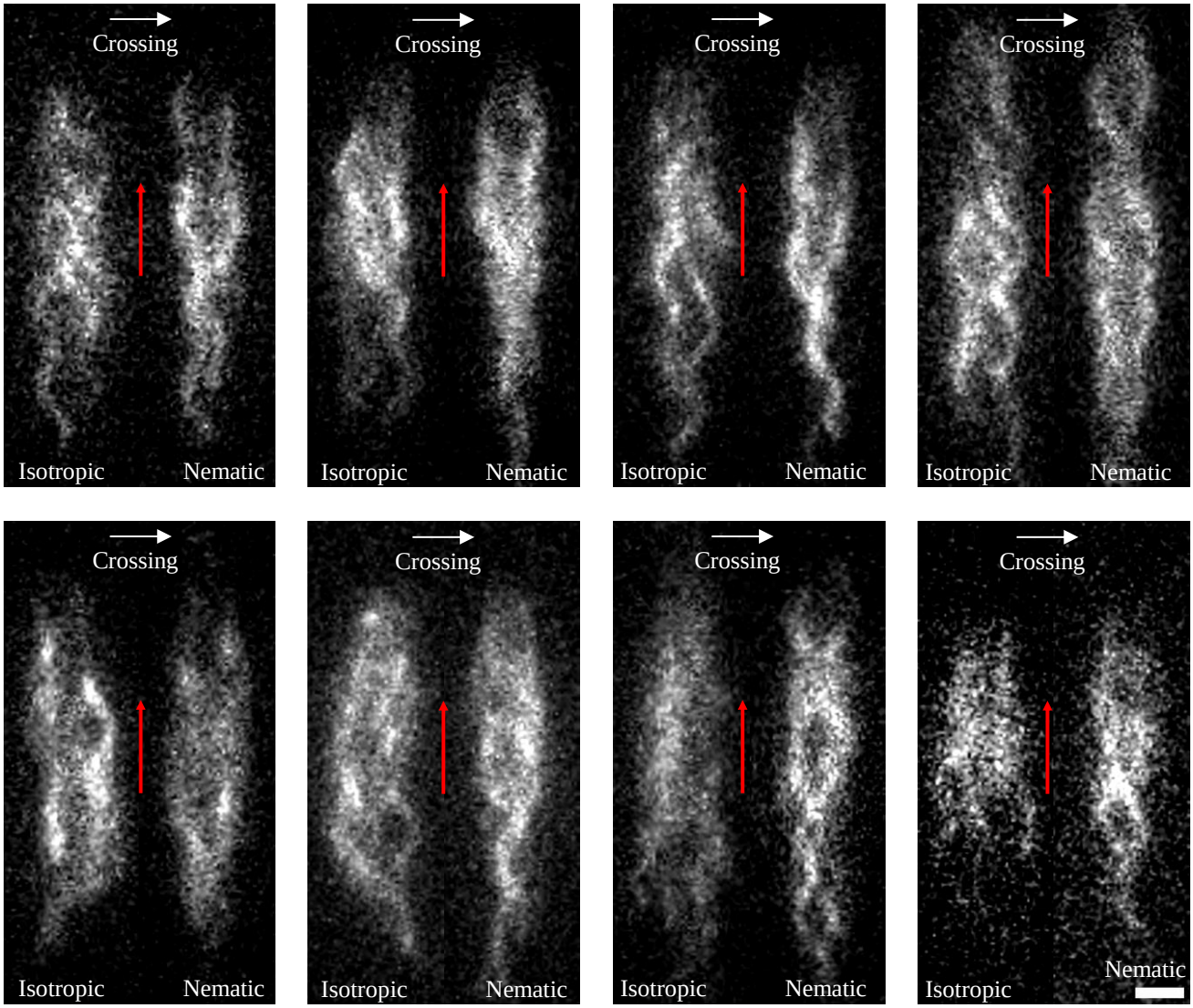

Figure S12: Eight representative images of the bacterial flagella before and after crossing the isotropic-nematic interface. The red arrow indicates the swimming direction. Scale bar = 2 μm

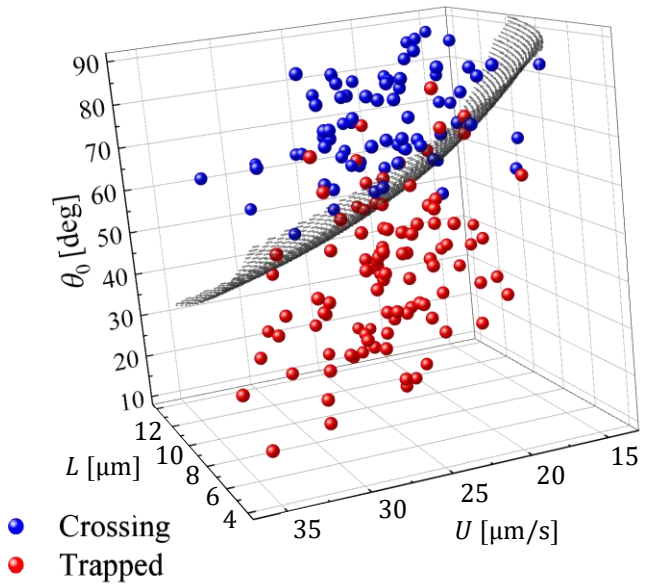

Figure S13: Experimental data (scattered symbols) and our theoretical prediction (a plane) in 3D space: L, U, and θ_0. The blue and red symbols correspond to the crossing and trapped bacteria at the interface, respectively. The black dotted plane is a theoretically predicted boundary, where $\Delta_{\text{int}} = 1$ μm.